1 **Novel structure and composition of the unusually large germline determinant of**

2 **the wasp Nasonia vitripennis**

3

4 Allie Kemph[1], Kabita Kharel[2], Samuel J. Tindell[2],

5 Alexey L. Arkov[2]* and Jeremy A. Lynch[1]*

6

7 1 Department of Biological Sciences, University of Illinois at Chicago, Chicago, IL 60607

8 2 Department of Biological Sciences, Murray State University, Murray, KY 42071

9

10 *Correspondence: jlynch42@uic.edu, aarkov@murraystate.edu

11

12 **Abstract**

13   Specialized, maternally derived ribonucleoprotein (RNP) granules play an

14 important role in specifying the primordial germ cells in many animal species. Typically,

15 these germ granules are small (~100 nm to a few microns in diameter) and numerous;

16 in contrast, a single, extremely large granule called the oosome plays the role of

17 germline determinant in the wasp Nasonia vitripennis. The organizational basis

18 underlying the form and function of this unusually large membraneless RNP granule

19 remains an open question. Here we use a combination of super-resolution and

20 transmission electron microscopy to investigate the composition and morphology of the

21 oosome. We show that the oosome has properties of a viscous liquid or elastic solid.

22 The most prominent feature of the oosome is a branching mesh-like network of high

23 abundance mRNAs that pervades the entire structure. Homologs of the core polar

24 granule proteins Vasa and Oskar do not appear to nucleate this network, but rather are

25 distributed adjacently as separate puncta. Low abundance RNAs appear to cluster in

26 puncta that similarly do not overlap with the protein puncta. Several membrane-bound

27 organelles, including lipid droplets and rough ER-like vesicles, are incorporated within

28 the oosome, whereas mitochondria are nearly entirely excluded. Our findings show that

29 the remarkably large size of the oosome is reflected in a complex sub-granular

30 organization and suggest that the oosome is a powerful model for probing interactions

31   between membraneless and membrane-bound organelles, structural features that

32   contribute to granule size, and the evolution of germ plasm in insects.

33

34   **Background**

35   Primordial germ cells are generally specified early in development to prevent

36   somatic differentiation and ensure the successful production of gametes. In many

37   sexually reproducing organisms, germ cells are among the first to be specified via their

38   uptake of a specialized cytoplasm consisting of maternally deposited mRNAs and

39   proteins, termed 'germ plasm' [1]. The germ plasm is typically characterized by

40   numerous membraneless complexes that are highly concentrated in mRNA and RNA-

41   binding proteins called germ granules. While there is significant variability in the

42   contents of these granules [2, 3], there are some highly conserved factors including

43   mRNAs encoding *nanos* homologs, and conserved core proteins of the Vasa-Ddx4,

44   Tudor, and Argonaute-Piwi families [4]. The germ plasm nucleator varies across

45   species, but these proteins often share intrinsically disordered regions (IDRs) believed

46   to play an important role in driving liquid-liquid phase separation [5-7].

47   Among holometabolous insects, germ plasm nucleation is dependent upon the

48   gene *oskar* and its loss correlates with shifts to the alternative zygotic induction

49   specification strategy [8]. *osk* was originally only detected in the dipteran lineage where

50   it has been studied extensively in the model organism *Drosophila melanogaster* [9, 10].

51   An *osk* ortholog was eventually discovered in the wasp *Nasonia vitripennis*, where it

52   was shown to have a conserved (if highly modified) role in germ plasm nucleation [8].

53   More recently it was found that *osk* arose early in insect evolution and originally played

54   no role in germline determination [11-13]. In both *Drosophila* and *Nasonia, osk* mRNA

55   localizes to the posterior pole during oogenesis, where it is translated and functions

56   upstream of the other core assembly proteins Vasa and Tudor [8, 14]. In *Drosophila*,

57   these proteins form many small 500nm ribonucleoprotein complexes called polar

58   granules, phase-transitioned particles with both liquid and hydrogel-like properties [15].

59   These granules bind, protect, and regulate the expression of germline mRNAs. With the

60   advent of super-resolution imaging techniques, it has emerged that polar granule-

61 localized mRNAs accumulate in distinct homotypic clusters in the context of these

62 protein-based granule [16, 17].

63 In stark contrast, the germ plasm of *Nasonia* takes the form of a single large

64 particle, forty-fold larger than the individual polar granules. How this unusually large

65 size for a membraneless intracellular structure is achieved and maintained is of very

66 high interest. We have previously shown that the mRNA profile of the oosome is quite

67 different from the polar granules, only sharing a handful of mRNA molecules [3]. Our

68 recent examination of the protein composition and arrangement of the oosome revealed

69 granules of Osk/Vasa/Aubergine that are similar in size to polar granules distributed

70 throughout the oosome [18]. However, they showed limited colocalization suggesting

71 that they do not form the same type of structures as the polar granules. In addition we

72 found that Tudor protein forms a novel shell-like distribution around the surface of the

73 oosome, which has no counterpart in the fly [18].

74 Several unanswered questions about the structure and composition of the

75 oosome still remain, that we begin to address here. First, we explore the development

76 of its shape throughout the pre-blastoderm stage to gain insights into its behavior and

77 biophysical properties. Additionally, since the nucleation of homotypic clusters of

78 mRNAs is a major, functionally important feature of polar granules, we explore how

79 mRNAs of different enrichment levels are distributed in the oosome relative to each

80 other, and to the core protein components. Finally, due to the pronounced enrichment of

81 mitochondria in *Drosophila* germ plasm [19], and the demonstrated importance of

82 membrane-bound organelles in regulating polar granule morphology [20], we've also

83 examined the distribution of subcellular components in and around the oosome. Our

84 analyses identified a clear pattern in oosome morphology, unexpected organelle

85 interactions, and revealed a novel arrangement of germ plasm mRNAs.

86

87 **Results**

88 *Dynamic oosome morphology during early embryogenesis*

89 We previously observed that the oosome underwent dramatic changes and

90 migration in the early embryo prior to cellularization [8]. We examined oosome behavior

91 during this period which encompasses the first 3 hours of development, comprising the

92   first seven syncytial nuclear divisions and most of the pre-blastoderm stage prior to pole

93   cell budding, to gain insights into the material properties of the oosome and the forces

94   acting upon it. For the first hour of development, the oosome is attached to the posterior

95   cortex (Figure 1A), where it was assembled during oogenesis. After the maturation of the

96   female pro-nucleus and the first syncytial nuclear division, the oosome detaches and

97   migrates anteriorly as far as 50% egg length through nuclear cycles 2 and 3. The oosome

98   then moves posteriorly in cycles 4 and 5, until it reassociates with the cortex during the

99   sixth syncytial nuclear division. It finally becomes flattened against the posterior cortex

100   during the seventh cycle, just before naïve nuclei arrive and pole cell budding initiates

101   (Figure 1A).

102   Oosomes from each nuclear division cycle were imaged with spinning-disc

103   confocal microscopy at high z-resolution using fluorescent probes against the abundant

104   and ubiquitous *Nv-osk* transcript to delineate the borders of the oosome. Surfaces were

105   generated around the reconstructed oosome projections and were measured for

106   sphericity. We suspect that the combination of the forces driving the oosome's migration,

107   together with resistance to this force by remaining cortical attachments are responsible

108   for the deformation of the oosome into complex irregular shapes with low sphericity

109   observed in NC0 as the oosome begins detaching from the posterior cortex (Figure 1B &

110   C). Once the oosome is completely detached from the cortex, it exhibits gradually

111   increasing sphericity as it is suspended in the central column of the embryonic cytoplasm.

112   This behavior is indicative of relaxation to minimize surface tension, which is a property

113   of either a viscous liquid or an elastic solid [21, 22]. Finally, as the oosome is pushed back

114   against the posterior cortex it flattens and spreads into a lens-like shape (Figure 1B & C),

115   resembling membrane wetting behavior of a liquid droplet [23] or the deformation of an

116   elastic solid. Taken together, the dynamic morphology of the oosome throughout the pre-

117   blastoderm stage suggest that it displays properties of either a viscous liquid or an elastic

118   solid. The development of fluorescently tagged proteins and associated methods like

119   FRAP in *Nasonia* will be required to make a final determination of the physical properties

120   of the oosome.

121

122   *Distribution of mRNAs within the oosome*

123   *Drosophila* germ plasm contains polar granules which include at least two distinct
124   ribonucleoprotein complexes: germ granules and founder granules [17, 24], The latter are
125   responsible for the decay of germ plasm-localized *osk* mRNA, which is toxic for pole cell
126   development [24]. The germ granules are the major functional component of the
127   *Drosophila* germ plasm. They consist of a conserved core set of proteins (Osk, Vas, Tud,
128   and Aub) that are distributed throughout each granule in complex patterns of more or less
129   colocalization [16, 25, 26]. The protein core is decorated by homotypic clusters of mRNAs
130   which occupy specific positions within the granule that are correlated with their expression
131   levels [16, 17, 27].

132   The core protein components of the germ granules are conserved as constituents
133   of the oosome in *Nasonia*. Our recent super-resolution imaging of the pre-blastoderm
134   oosome revealed that Nv-Osk, Nv-Vas, and Nv-Aub accumulate in only partially co-
135   localized puncta that are distributed throughout the oosome (Fig 2B" & C") [18]. Nv-Tud
136   differs in that it is highly concentrated around the oosome periphery, with some puncta
137   dispersed interiorly (Figure 2A") [18]. Whether this distinct protein arrangement impacts
138   the distribution of the dozens of transcripts that are localized to the oosome remains
139   unknown [3].

140   To address this gap, we selected four oosome-localized transcripts – *Nv-oskar (Nv-*
141   *osk)*, *Nv-barkbeetle (Nv-bark)*, *Nv-innexin*, and *Nv-qin* for super-resolution fluorescent *in*
142   *situ* hybridization. *Nv-osk* and *Nv-bark* are two of the most highly enriched transcripts in
143   the oosome and are expressed at levels an order of magnitude higher than typical
144   oosome genes, represented by *Nv-qin* and *Nv-innexin* [3]. The high abundance
145   transcripts *Nv-bark* and *Nv-osk* are distributed in apparently overlapping mesh-like
146   networks that pervade the oosome (Figure 2A, 2A', & 2A'''). There appear to be regions
147   of relatively high, and relatively low intensity along those networks, indicating a variable
148   intensity in clustering of these mRNAs. Such pattern has not been reported to our
149   knowledge in other germ granules where homotypic clustering of mRNAs has been
150   observed. In contrast, the lower abundance transcripts (*Nv-qin* and *Nv-innexin)* cluster
151   into distinct puncta that are distributed relatively diffusely within the oosome and appear
152   to be juxtaposed with the *Nv-osk/bark* network (Figure 2B, B', C, & C').

153   To quantify our qualitative observation about the relative positions of the four
154   transcripts with respect to one another, we performed colocalization analyses of each
155   transcript relative to the *Nv-osk* network. To determine the upper limit of co-localization
156   for our analysis we labeled *Nv-osk* with a mix of stellaris CALFluor®Red 590-labelled
157   probes and Quasar®670-labelled probes and measured a PCC of 0.87± 0.03 (Figure 2D).
158   *Nv-osk* and *Nv-bark* highly co-localize within the oosome with a PCC of 0.71 ± 0.05, where
159   they appear to co-label a mesh-like network running throughout the oosome interior
160   (Figure 2A''' & D). The punctate *Nv-innexin* and *Nv-qin* only weakly co-localize with *Nv-*
161   *osk* with a PCC of 0.16 ± 0.05 and 0.13 ± 0.05, for *Nv-qin* and *Nv-innexin* respectively
162   (Figure 2B-D). *Nv-innexin* and *Nv-qin* also show no co-localization with each other with a
163   PCC of 0.05± 0.0, supporting the presence of homotypic RNA clustering in the oosome
164   (Figure 2E).

165   We next investigated how these transcripts interact with the protein components
166   of the oosome. As previously described, Nv-Osk and Nv-Vasa, are distributed as relatively
167   diffuse puncta throughout the oosome, while Nv-Tud is highly concentrated at the oosome
168   surface (Figure 2A'', B'', & C'') [18]. Neither Nv-Osk (PCC of -0.02± 0.03), nor Nv-Vasa
169   (PCC of 0.02± 0.03) showed any co-localization with the *Nv-osk* mRNA network (Figure
170   2B, C, & F). Nv-Tud showed only weak co-localization (PCC of 0.11 ± 0.04), which may
171   reflect a greater likelihood of the continuous network of Nv-Tud to intersect or overlap with
172   the extensive network of *Nv-osk* (Figure 2A'''&D). Surprisingly, we found that the punctate
173   mRNAs *Nv-innexin* and *Nv-qin* also showed no co-localization with these internal protein
174   granules (Figure 2F). Both *Nv-innexin* and *Nv-qin* are maintained in *Nasonia* pole cells
175   and their lack of co-localization suggests these internal Nv-Osk/Vasa granules are not as
176   essential as germ granules in transcript germ plasm localization and transport to pole
177   cells [3].

178   Non-homogenous RNA distribution is a common feature in germ granules and our
179   results thus far suggest that is also the case in *Nasonia*. The arrangement of RNA into
180   homotypic clusters has been described in germ granules of several model organisms
181   (*Drosophila*, *C. elegans* and zebrafish) [2, 16, 17, 28, 29], and the punctate organization
182   and lack of co-localization of *Nv-innexin* and *Nv-qin* support the existence of these
183   clusters within the oosome as well (Figure 2B', C', & E). Although our co-localization

184 results suggest that *Nv-osk* and *Nv-bark* appear to be distributed along the same network

185 (Figure 2D), they may still form distinct clusters that cannot be resolved with our current

186 optical capabilities. Indirect evidence for this is our previous observations that *Nv-osk*

187 mRNA is rapidly degraded in the pole cells [8], while *Nv-bark* remains at high levels in the

188 primordial germ cells throughout embryogenesis [3]. We have observed that this

189 difference in regulation is apparent much earlier in the oosome, with *Nv-osk* signal

190 showing significant reduction in the intact oosome prior to pole cell formation (Figure S1).

191

192 *Fragmentation and stability of the oosome*

193 In most species, germ plasm consists of many small amorphous ribonucleoprotein

194 particles that are of a relatively uniform size (often less than a few micrometers) [30, 31],

195 but granule size can increase both naturally over time through fusion events [31]. as well

196 as artificially through protein knockdown [20, 32]. For example the MEG-3 protein clusters

197 that form a shell around P granules in *C. elegans* are hypothesized to act as a Pickering

198 agent, which is supported by the finding that MEG-3 knockdown results in fewer, larger

199 granules [32]. The oosome somehow naturally bypasses the size constraints generally

200 observed in germ granules forming a uniquely large germ plasm complex. Previous

201 observations showed that the disruption of Tudor, which forms a shell around the oosome

202 (Figure 2A", [18]) results in smaller oosomes [8], suggesting that Tudor may stabilize the

203 large size of the oosome, which contrasts with the role of the shell surrounding P granules.

204 In addition to the singular large oosome, we found smaller aggregates of germ

205 plasm material at the posterior pole, which we named satellite particles. The composition

206 of these satellite particles appears to be identical to the oosome. The network of *Nv-*

207 *osk/bark* mRNA punctuated with scattered spots of lower abundance RNAs and core

208 proteins (e.g., Nv-Osk, Nv-Vasa) also appears to be maintained (Figure 3A & B).

209 Investigating the origin and fate of these satellite particles and the oosome should provide

210 insights into the mechanisms governing germ granule size.

211 Satellite particles are variable in size, ranging from similar in size to polar granules

212 to others nearly as large as the oosome, with a continuum of intermediate sizes between

213 those extremes. The number of satellite particles was variable across embryos, however,

214 within that variability we could detect a clear trend of decreasing satellite particle count

215   over developmental time (Figure 3C). The decreasing number of satellite particles
216   suggests they are either fusing together and with the main oosome over time, or that the
217   smaller particles are dissolving in the bulk cytoplasm. We cannot currently distinguish
218   between these possibilities.

219   Another open question is the origin of the satellite particles. Their significantly
220   higher numbers in the earliest division cycles suggests that they either assemble
221   concurrently with the oosome during oogenesis, or that they arise through fragmentation
222   of the oosome under the strong deforming forces that are acting upon it at this stage
223   (Figure 1). In the case of the larger particles, a subset we have termed sub-oosomes
224   (volume 20% or greater than the main oosome), we propose that they are primarily the
225   result of fragments breaking free from the main oosome, and that these in large part re-
226   fuse with the oosome in later stages. In support of this proposal, sub-oosomes are found
227   with the highest frequency in the earliest nuclear cycles and most closely resemble
228   oosome architecture and have even been observed to share the distinct Tudor-shell
229   distribution (Figures 3D, E & S2A'). Further, we observe putative intermediate cases in
230   the earliest nuclear cycles where a large fragment of the oosome is only tenuously
231   connected to the rest and appears to be in the process of detaching to form a sub-oosome
232   (Movie S2).

233

234   _Ultrastructural analysis of the oosome_

235   Our fluorescence based analyses have suggested that the underlying structure of
236   the oosome may be more heavily RNA based than _Drosophila_ germ granules [20], and
237   perhaps germ granules from other species. To gain a higher resolution understanding of
238   the structure of the oosome, we examined it with transmission electron microscopy
239   (TEM). The main substance of the oosome appears to be an electron-dense fibro-
240   granular network with pockets of lower electron density material distributed throughout
241   (Figure 4A-A'). This arrangement is strikingly reminiscent of the mesh-like organization of
242   the highly enriched mRNAs _Nv-bark_ and _Nv-osk_ surrounding areas of low to no signal
243   (Figures 2A''' & 4A'). This further suggests that the underlying architecture of the oosome
244   is composed primarily of a mesh-like network of RNA.

245   Germ granules are associated with membrane-bound organelles in multiple
246   species [33, 34], and TEM revealed that the oosome conforms to this broad pattern. Most
247   immediately evident are the putative lipid droplets concentrated to the periphery of the
248   oosome as well as frequently within it (Figure 4A"). There are no identifiable Golgi-like
249   structures, nor are there canonical tubular or sheet-like endoplasmic reticulum structures.
250   However, we did observe spherical membrane-bound organelles studded with what
251   appear to be ribosomes that were distributed both within the oosome and throughout the
252   bulk cytoplasm. These are highly reminiscent of the newly defined ER-like organelle
253   compartment called Ribosome-Associate Vesicles (RAVs) (Figure 4A" white arrowheads)
254   [35]. These were recently described in secretory cell lines and have retroactively been
255   identified in various organisms and across different cell types [35]. Although they have
256   not previously been observed in embryonic germ plasm, similar structures (termed RER
257   vesicles) were described in the "pseudo-pole plasm" in the ovary of an earwig
258   (Dermaptera) [36, 37], These ribosome-associated vesicles have been proposed to
259   transport active ribosomes to distal neurites to promote local translation [38]. Although it
260   is unclear if this role in promoting local translation extends to the context of the large,
261   dense structure of the oosome.

262   Surprisingly, we found very little association between the oosome and
263   mitochondria. Mitochondria are occasionally seen adjacent to the oosome, and almost
264   never within it. They do not appear to be enriched in any way around the oosome. This
265   differs from *Drosophila melanogaster,* where mitochondria are strongly enriched around
266   polar granules, and are often in direct contact. This may suggest alternative energy
267   requirements or sources between the oosome and polar granules. To confirm and expand
268   on these observations we next visualized both structures within and around the oosome
269   using fluorescence microscopy.

270

271   *Interactions of the oosome with membrane-bound organelles*

272   Although RAVs have not been found in embryonic germ plasm of any other animal
273   species, *Drosophila* polar granules have been found to contact conventional endoplasmic
274   reticulum [20, 39]. To further validate that the unusual vesicles we see in the *Nasonia*
275   oosome and surrounding cytoplasm are related to the ER, and thus likely to be RAVs as

276   recently defined [35], we used an antibody against the KDEL peptide. This sequence is a

277   highly conserved feature of ER resident proteins throughout animals that is commonly

278   used to characterize ER shape and distribution. KDEL-labelled structures were punctate

279   (Figure 5B-B'), consistent with the appearance of RAVs when observed with fluorescent

280   microscopy [35]. Consistent with the vesicles observed by TEM (Figure 4A" and 5A),

281   these punctate KDEL positive structures were also widely distributed throughout the

282   oosome and the surrounding cytoplasm (Figure 5B-B'). To determine if RAVs were

283   enriched in the oosome relative to the general cytoplasm we compared RAV count in

284   segmented regions within and just outside of the oosome. We found no significant

285   difference in RAV number between the oosome and the surrounding cytoplasm (Figure

286   5C).

287   Unlike RAVs, while mitochondria were also apparent in the surrounding cytoplasm

288   and at the oosome periphery, they appeared to be excluded from the oosome (Figures

289   4A"&5D). To further validate this observation, we used the marker ATP5A to fluorescently

290   label mitochondria and again compared the count in segmented regions both within and

291   just outside of the oosome (Figure 5E-F). Consistent with our TEM observations, there

292   are significantly fewer mitochondria inside the oosome than in the surrounding cytoplasm

293   (Figure 5F). This finding is unexpected as germ plasm is generally enriched in

294   mitochondria [30, 40, 41]. In *Drosophila*, the long isoform of Oskar, which is absent in

295   *Nasonia* [8], is responsible for anchoring mitochondria at the posterior cortex [19]. The

296   observed lack of mitochondrial enrichment suggests there is no equivalent mechanism

297   for concentrating mitochondria in the region of pole cell formation in *Nasonia.* In fact, we

298   suspect that the opposite may be the case. At later stages, mitochondria are highly

299   concentrated around the pre-blastoderm syncytial nuclei (Figure 5G). When the

300   presumptive pole cell nuclei enter the oosome at the pole cell budding stage, the vast

301   majority of the mitochondria are removed from the nuclear periphery (Figure 5H' and

302   Movie S1). Based on these observations, the oosome may play a role in establishing a

303   bottleneck of mitochondria at the very beginning of germline establishment and may thus

304   be important in maintaining mitochondrial quality over generations.

305   Taken together, these findings show that while the oosome does contact and

306   incorporate organelles into its internal network structure, there is some unknown means

307   of discrimination whereby mitochondria are excluded. Further experiments are necessary

308   to understand how mitochondria are excluded, and whether RAV incorporation is a

309   passive part of oosome assembly or if it may play a functional or structural role.

310

311   **Discussion**

312   Our analysis of the structure and composition of the oosome revealed numerous

313   novel and unexpected features that highlight the striking diversity in membraneless

314   organelle form. By investigating this exceptionally large and active germ plasm complex

315   found in *Nasonia*, we broaden our understanding of which structural features may

316   contribute to the stability of large condensates and of germ plasm evolution in insects.

317

318   *mRNA clustering in the oosome*

319   Over the last several years, self-sorting of RNAs into homotypic clusters within

320   germ granules has emerged as a surprisingly well conserved feature of germ granules

321   across animal phyla [16, 17, 28, 29]. Our results partially conform to this trend, and

322   potentially extend the forms homotypic RNA interactions can take. The scattered

323   punctate distribution and lack of co-localization of low and moderately enriched mRNAs

324   like *Nv-innexin* and *Nv-qin* is strongly suggestive of homotypic clustering of mRNA

325   within the oosome environment (Figure 2B', C', &E). In *Drosophila*, mRNAs accumulate

326   into homotypic clusters only in the context of core germ granules (composed largely of

327   Osk and Vas protein) [27]. In contrast, the *Nv-qin* and *Nv-innexin* puncta do not appear

328   to form in the context of a Nv-Osk and Nv-Vas complex. Rather they are scattered along

329   an apparent network of highly enriched mRNAs of *Nv-bark* and *Nv-osk*.

330   The network distribution of *Nv-osk* and *Nv-bark* does not preclude homotypic

331   interaction of these mRNAs. Indeed, the degree of colocalization between *Nv-bark* and

332   *Nv-osk* is quite high (PCC=0.71), but somewhat lower than the value for the

333   colocalization for two *Nv-osk* probe sets (PCC=0.87) (Figure 2D). This suggests that

334   any overlap may be partial, and we cannot exclude that the apparent colocalization is a

335   result of extremely high concentration of these molecules in a constrained area. To

336   distinguish whether the *Nv-bark* and *Nv-osk* mRNA networks are truly largely

337   overlapping, or whether they are actually distinct and potentially homotypic networks,

338   methods that can further enhance the ability to resolve these tightly packed molecules,

339   such as expansion fluorescence *in situ* hybridization (ExFISH), will be required [42].

340

341   *Potential origin and functional significance of the mesh-like mRNA network*

342   Unlike the discrete puncta of moderately enriched mRNAs, the large-scale,

343   mesh-like network distribution of *Nv-osk* and *Nv-bark* is not a pattern previously

344   observed for embryonic germ granule mRNA. However, it was recently found that

345   during late oogenesis in *Drosophila*, *oskar* particles "stick" together forming larger

346   agglomerates [43]. While these are not on the scale of the oosome network, it does

347   indicate the propensity of *oskar* particles to adhere to each other. This suggests the

348   presence of a mechanism in *Nasonia*, potentially involving its close association with *Nv-*

349   *bark* mRNA, further stabilizes these interactions allowing the formation of this large

350   network. Additionally, a recent large scale RNAi screen in *Drosophila* identified nine

351   endoplasmic reticulum (ER), nuclear pore complex (NPC), and cytoskeleton related

352   proteins whose knockdown resulted in branched mesh-like morphology of polar

353   granules, demonstrating the capacity of these granules to also form similarly shaped

354   networks [20]. Considering the shared core assembly proteins between polar granules

355   and the oosome, further investigation into how the oosome interacts with the ER, NPC,

356   and cytoskeleton and how this compares with polar granules may provide insight into

357   the evolution of its novel form.

358   In *Drosophila*, *osk* mRNA is toxic to pole cells and undergoes targeted

359   degradation prior to and during pole cell formation [24]. The specificity of *osk*

360   degradation appears to arise from its segregation into separate germ granules called

361   founder granules, which associate with decapping and degradation factors [24]. In

362   *Nasonia,* it has been shown that *Nv-osk* is similarly rapidly cleared from pole cells [8].

363   and we expand on this finding to show that *Nv-osk* mRNA levels begin to decrease

364   significantly during embryogenesis shortly before pole cell budding (Figure S1). This

365   finding further supports that removing *osk* ortholog mRNA is a conserved requirement

366   for germ cell development in insects. However, our results revealed no indication that

367   there is a clear equivalent to the founder granules that specifically segregate *Nv-osk*

368   mRNA, which is distributed at high levels in a network throughout the oosome. This

369   network does not appear to be correlated with early mRNA degradation, as we found a

370   high degree of co-localization with at least one other mRNA, *Nv-bark* (Figure 2D) which,

371   unlike *Nv-osk*, is maintained at high levels beyond pole cells through to the late

372   embryonic gonads [3]. Thus, there is likely to be a distinct mechanism for regulating *Nv-*

373   *osk* mRNA.

374   The degradation of *osk* precedes the destabilization and disassembly of founder

375   granules in pole cells [24]. The conserved timing of significant *Nv-osk* degradation

376   shortly before and during pole cell formation (Figure S1) [8], suggests a potentially

377   similar mechanism for the oosome disassembly that occurs during pole cell formation to

378   allow germ plasm partitioning. Future work to determine if the *Nv-osk* RNA network

379   plays a structural role in the oosome will require more sophisticated techniques than

380   currently available in *Nasonia*, as we cannot currently isolate early roles in nucleating

381   the oosome during oogenesis from a later role in stabilizing the large granule. Nor can

382   we clearly disentangle a structural role of the mRNAs from those of their presumed

383   protein products since RNAi will affect both.

384

385   *Oosome-organelle interactions*

386   Germ granules are known to associate with membrane-bound organelles [33,

387   34]. In fact, Balbiani bodies, another germline RNP complex found in immature oocytes

388   and comparable in size to the oosome (10-100 µm), encompass many membrane-

389   bound organelles such as the endoplasmic reticulum, Golgi and especially

390   mitochondria. Therefore, we were unsurprised in our TEM imaging of the oosome to find

391   that it does contain many membrane-bound organelles (Figures 4 and 5A-C).

392   Conversely, the striking lack of mitochondria was unexpected (Figure 5D-F).

393   Mitochondria are generally enriched in germ plasm to facilitate maternal inheritance, a

394   process which is mediated by the long isoform of Oskar in *Drosophila* [19]. Since this

395   long Oskar isoform is absent from *Nasonia* [8], we initially suspected an alternative

396   enrichment mechanism exists in the wasp's oosome, or posterior polar region. However,

397   while mitochondria seem to be distributed around the cortex of the embryo and around

398   the syncytial nuclei (Figure 5G), they seem to be nearly completely excluded from the

399   oosome, even as it begins incorporating nuclei (Figure 5H & Movie S1). Given that other

400   organelles, even larger ones like nuclei and lipid droplets, seem to be easily

401 incorporated into the oosome (Figure 4), we propose that the oosome is selectively

402 permeable to organelles and some unknown mechanism exists within the oosome that

403 specifically prevents mitochondrial incorporation. Further imaging of how mitochondria

404 interact with the oosome both during assembly, budding, and pole cell formation would

405 provide a more comprehensive view of this mechanism.

406 The inclusion of ribosome-associated vesicles (RAVs) in the oosome was also

407 unexpected since they had not yet been described in insect embryos, although they are

408 suspected to be widespread across different tissue and cell types [35]. A recent study

409 found that RAVs promote local translation in secretory cells by transporting active bound

410 ribosomes [38]. Active translation has been observed previously in germ granules [44,

411 45], but it is still unknown whether translation occurs within the oosome specifically, and

412 whether RAVs are involved in translational regulation. These questions will be

413 addressed by future studies investigating post-transcriptional regulation within the

414 oosome.

415

416 *Material properties of the oosome*

417 How the unique compositional features of the oosome are reflected in its material

418 properties is difficult to directly probe without the establishment of live imaging in

419 *Nasonia*. We did, however, gain some insight from identifying patterns which can be

420 attributed to specific oosome behaviors in response to the external forces that drive its

421 migration. The most irregularly shaped oosomes are found immediately after egg lay

422 when it is initially still attached to the cortex, they become more spherical during

423 migration, and finally flatten upon re-establishing contact with the posterior cortex

424 (Figure 1B & C). These patterns suggest that the oosome is at least partially liquid-like

425 as it deforms and does not hold a specific shape under pressure, relaxes into a more

426 spherical shape upon release from this pressure, and wets the posterior cortex upon

427 reassociation (Figure 1). Furthermore, just before budding, the oosome coats incoming

428 nuclei displaying additional wetting behavior and a potential model for the incorporation

429 of other oosome-associated organelles (Movie S1). Additionally, the diminishing

430 satellite particle count supports a more transient liquid-like particle regardless of

431 whether it occurs by dissolution or fusion (Figure 3C), both of which have been

432 previously observed in a germ granule context in the liquid-like P granules in *C. elegans*

433 [31]. Although these observations suggest that the oosome is more liquid-like, we

434 cannot currently dismiss the possibility that the oosome may be hydrogel-like or a

435 combination of the two. Condensate material properties are often more complex than a

436 single feature and can even be multiphasic as is the case for P granules which have a

437 liquid-like PGL protein core [31], stabilized by surrounding gel-like MEG-3 clusters [46].

438

439 **Conclusion**

440 This work has identified several unique and unexpected features of the oosome.

441 Some provide plausible explanations for how the oosome maintains its unusually large

442 size and complexity, for example the branching network of *Nv-osk* and *Nv-bark* mRNA

443 running throughout the oosome. Others give potential insights into the functional

444 significance of the oosome, such as the presence of RAVs. Further research along

445 these lines will provide valuable insights into the assembly and function of

446 membraneless organelles in general. In addition, the complexity and investment of a

447 very high concentration of biopolymers localized to the oosome raises the question of

448 what the evolutionary significance of the oosome structure is. It seems to be a

449 conserved feature of the superfamily Chalcidoidea to which *Nasonia* belongs, as it has

450 been described from several genera spanning the most distantly related lineages [13,

451 47, 48]. Comparing the composition and structure of oosomes within this group could

452 provide unique insights into the evolutionary aspects of membraneless organelles at

453 different time scales.

454

455 **Methods**

456

457 Embryo collection and fixation for in situ hybridization and immunofluorescence

458

459 Adult females were allowed to lay eggs on *Sarcophaga bullata* pupae at 25 ºC for 3.5

460 hours in a modified petri dish apparatus called a Waspinator [49]. Host puparia were

461 then cracked and *Nasonia* embryos were transferred directly to a fixation solution (5 mL

462 heptane, 2 mL 10% methanol-free formaldehyde) and fixed overnight at room

463 temperature. Apart from embryos labeled with Nv-Tud, which were fixed for 2 hours at

464 room temperature and then overnight at 4°C. After fixation the vitelline membrane was

465 removed by affixing the membranes to double-sided tape, adding phosphate-buffered

466 saline with Tween (PBST), and then gently pushing with the flat edge of a 27-gauge

467 needle to release the embryo from the attached membrane as described previously

468 [50]. Fixed, devitellinized embryos were kept in PBST at 4°C for less than a week until

469 fluorescence *in situ* hybridization and/or immunofluorescence was performed.

470

471 Single-molecule FISH (smFISH)

472

473 Custom Stellaris RNA FISH oligonucleotide probe sets labelled with CALFluor590 or

474 Quasar670 were generated complementary to *Nv-oskar*, *Nv-innexin*, *Nv-qin* and *Nv-*

475 *barkbeetle*. Stellaris FISH was performed on devitellinized embryos following the

476 manufacturers protocol for *Drosophila* embryos (LGC Biosearch Technologies). Stellaris

477 RNA FISH was carried out for Figures 2 and 3 in tandem with immunofluorescence (IF),

478 where IF was performed first and followed by Stellaris FISH. After staining, embryos

479 were mounted under #1.5 glass coverslips in Fluoromount-G Mounting Medium with

480 DAPI from Southern Biotech.

481

482 Hybridization chain reaction (HCR) was utilized to label *Nv-osk* RNA for the preparation

483 of the oosome z-stacks used for sphericity and satellite particle measurements in

484 Figures 1 and 3, as well as to provide an oosome marker during the organelle staining

485 in Figure 5. We followed the Molecular Instruments dHCR v3.0 protocol for whole-mount

486 fruit fly embryos, with the *Nasonia*-specific modifications outlined by Taylor & Dearden,

487 2021 [51]. In images acquired for Figure 5 dHCR was performed first and followed by

488 immunofluorescence against KDEL or ATP5A. All embryos were mounted under #1.5

489 glass coverslips in Fluoromount-G Mounting Medium with DAPI from Southern Biotech.

490

491 Immunofluorescence

492

493   Immunofluorescence was carried out in combination with smFISH, either before

494   Stellaris, or after dHCR (see above). Devitellinized embryos were first washed 3 x 5 min

495   with PBS/0.1%TritonX-100 followed by 1 hour blocking in PBS.0.1%TritonX-

496   100/10%Western blocking reagent. Primary antibody incubation was at 4 ºC overnight.

497   Primary antibodies against core oosome proteins (Nv-Osk, Nv-Tud, and Nv-Vas) are

498   described in Kharel et al., 2024 [18], Antibodies against mitochondria (anti-ATP5A

499   antibody [15H4C4]) and endoplasmic reticulum (anti-KDEL antibody [EPR12668]) were

500   obtained from Abcam. Primary antibody concentrations were: 1:250 guinea pig anti-Nv-

501   Osk, 1:500 rabbit anti-Tud, 1:250 rabbit anti-Vas, 1:200 rabbit anti-KDEL, and 1:500

502   mouse anti-ATP5A. Embryos were then washed 3 times for 20 minutes in

503   PBS/0.1%TritonX-100, and then were blocked for 20 minutes in PBS/0.1%TritonX-

504   100/10% Western blocking reagent. Then incubation with Alexa Fluor 488-labeled

505   secondary antibodies (1:500) for 2 hours at room temperature. Finally, embryos were

506   washed five times for 20 minutes in PBS/0.1%TritonX-100. Stained embryos were either

507   mounted under #1.5 glass coverslips in Fluoromount-G Mounting Medium with DAPI

508   from Southern Biotech or underwent additional staining with Stellaris FISH (see above).

509

510   <u>Confocal microscopy and image processing</u>

511

512   Confocal imaging was performed using an Andor Revolution WD spinning disc

513   microscope with an Olympus inverted stand and 60x 1.4 NA silicon oil immersion

514   objective. Z-stacks for sphericity, satellite particle, and *oskar* mRNA intensity

515   measurements were acquired with an iXon 888 EMCCD camera in Andor Fusion

516   software at a scan size of 50 µm and an auto-step size of 0.22 µm. All other oosome

517   imaging were acquired with an additional 1.6x magnifier lens in the optical path. Super-

518   resolution images were obtained using the SRRF-Stream+ version 1.16.1.0 plugin to the

519   Andor Fusion software. Super-resolution radial fluctuations (SRRF) is an algorithm

520   which analyzes subpixel radial and temporal fluorescence intensity fluctuations across a

521   large number of frames acquired at the same position, to produce a single image with 2

522   to 6-fold increase in resolution obtainable by the 1MP iXon camera [52, 53]. All SRRF

523   images in this paper were acquired using 100 frames per image. Pixel shift correction of

524   multi-channel SRRF images was performed using 100 nm TetraSpeck microspheres as

525   alignment markers.

526

527   <u>TEM sample preparation and microscopy</u>

528

529   TEM embryos were collected from 0-1 hour egg lays, and initially fixed as described for

530   FISH. They were then devitellinized in PBS instead of PBST. They were then post-fixed

531   in 2%PFA/2.5%GA/0.1M Sodium Cacodylate pH 7.4 buffer for two hours at room

532   temperature followed by overnight at 4°C. These were then washed in sodium

533   cacodylate buffer (pH 7.2-7.4) and post-fixed in buffered 1% osmium tetroxide

534   for 2 hours. After several buffer washes, samples were dehydrated in an ascending

535   concentration of ethanol leading to 100% absolute ethanol, followed by 2 changes in

536   propylene oxide (PO) transition fluid. Specimens were infiltrated overnight in a 1:1

537   mixture of PO and LX-112 epoxy resin, and 2 hours in 100% pure LX-112 resin, and

538   then placed in a 60 C degree oven to polymerize (3 days). For better results, specimens

539   were embedded between 2 sheets of Aclar plastic (vs. traditional embedding molds),

540   regions of interest were etched out with a razor blade and glue-mounted onto blank

541   blocks for subsequent microtomy.

542

543   Semi-thin sections (0.5-1.0 µm) were cut and stained with 1% Toluidine blue-O to

544   confirm the areas of interest (via LM). Ultra-thin sections (70-80 nm) were cut using

545   a Leica Ultracut UCT model ultramicrotome, collected onto 200-mesh copper grids and

546   contrasted with 3% uranyl acetate and Reynolds lead citrate stains,

547   respectively. Specimen were examined using a JEOL JEM-1400 Flash transmission

548   electron microscope (operating at 80 kV). Micrographs were acquired using

549   an AMT Side-Mount Nano Sprint Model 1200S-B (and/or Biosprint 12M-B cameras),

550   loaded with AMT Imaging software V.7.0.1.

551

552   <u>Quantification of sphericity</u>

553

554 Oosome sphericity was measured for surfaces generated in Imaris around z-projections

555 of *Nv-osk* mRNA, which was fluorescently labeled with HCR FISH as described above.

556 Oosome projections were sorted into syncytial nuclear cycles 0-7 by counting nuclei

557 stained with DAPI, and 20 oosomes per cycle were analyzed to produce the sphericity

558 boxplot with significance relative to the earliest timepoint NC0 indicated. Significance

559 was determined with a Kruskal-Wallis test followed by a pairwise comparison with

560 Dunn's test. From the same pool of surfaces, 10 oosomes from each nuclear cycle were

561 randomly selected to display as a gallery plot generated in Imaris with sphericity values

562 depicted by color warmth.

563

564 Satellite particle counts

565

566 Satellite particle surfaces were generated in Imaris using the same *Nv-osk* mRNA z-

567 projections described for sphericity measurements. A standardized ROI of the embryo

568 posterior surrounding the oosome was captured with consistent acquisition settings.

569 Satellite particle counts and sub-oosome number were measured using the surfaces

570 generated in Imaris. Sub-oosome presence was identified manually and confirmed by

571 comparing surface volumes to identify satellite particles ≥ 20% of their corresponding

572 osome surfaces volume. Boxplots were generated from satellite particle count data for

573 each nuclear cycle, and significance relative to the earliest timepoint NC0 indicated.

574 Significance was determined with a Kruskal-Wallis test followed by a pairwise

575 comparison with Dunn's test. For each nuclear cycle, 20 embryos were analyzed for

576 both satellite particle count and sub-oosome presence.

577

578 Organelle count per ROI

579

580 Using Imaris software, regions of interest of 256x256 pixels were generated both within

581 and just outside of 10 oosomes, with dHCR labelled *Nv-osk* mRNA as an oosome

582 marker. Imaris spot detection was run within these segmented ROIs to label either

583 punctate KDEL or punctate ATP5A signal. A pairwise Wilcoxon rank sum test was then

584 carried out comparing spot detection within and just outside each oosome. Control

585 images of embryos stained using only secondary antibodies and no primary antibodies

586 detected no spots using the same acquisition and spot detection settings.

587

588 <u>Pearson's correlation coefficient (PCC) analysis</u>

589

590 PCC were determined using the Bioimaging and Optics Platform (BIOP) version of the

591 JACoP Plugin in Fiji [54]. An ROI was manually generated around each oosome in a

592 SRRF, pixel-shift corrected image. Automatic thresholding options were applied to

593 sample images and Otsu thresholding was identified as most accurately reflecting the

594 signal across all mRNAs and proteins and therefore applied to each image during co-

595 localization analysis. PCC outputs were averaged across oosomes for each condition

596 and used to generate bar graphs in Figure 2. Costes randomization [55] was applied to

597 each image to evaluate the significance of co-localization. The number of oosomes

598 analyzed for each pair were as follows: five for Osk/*innexin* and Vasa/*qin*; six for

599 *osk/osk*, *osk/bark*, Osk/*qin*, and Vasa/*innexin*; eight for *innexin/innexin* and *innexin/qin;*

600 eleven oosomes for *osk/qin*, *osk*/*innexin*, *osk*/Vasa, and *osk*/Osk; and twelve for

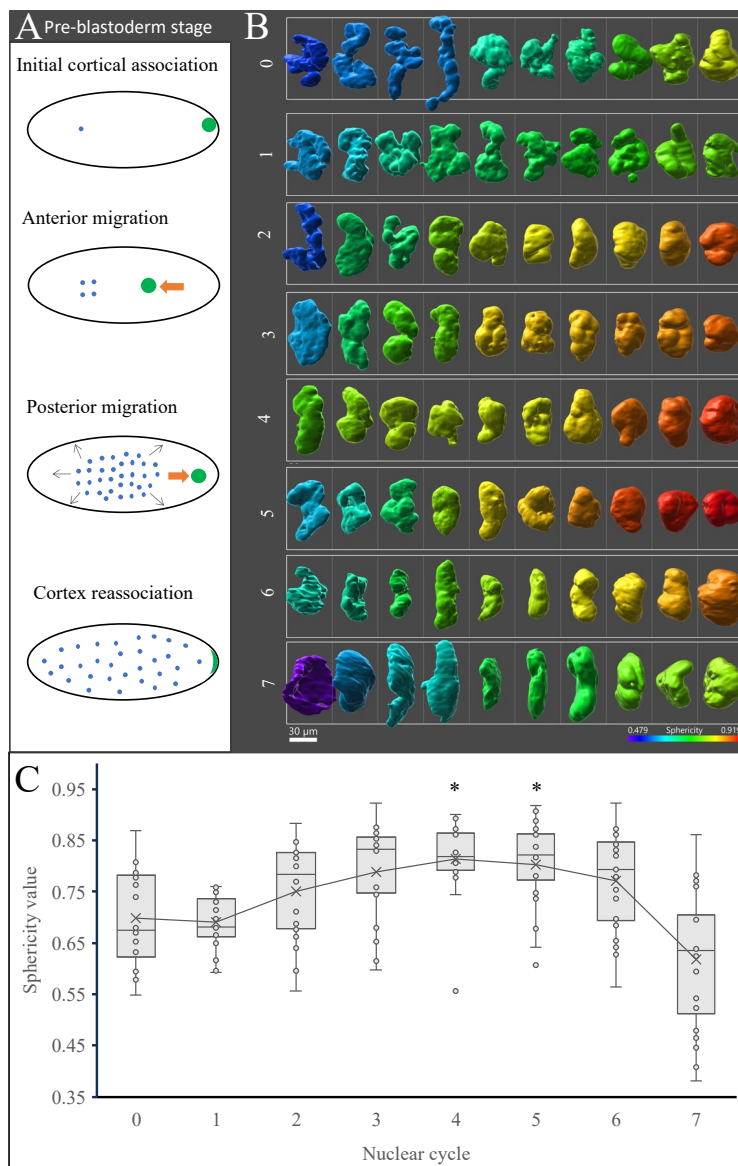601 *osk*/Tud.

602

603 **Figures:**

604

Figure 1: Oosome morphology is dynamic with lower sphericity at cortical association than throughout migration. (A) A diagram of oosome behavior during the pre-blastoderm stage. The oosome is shown in green and nuclei in blue. The orange arrow indicates the direction of oosome migration, and the grey indicates nuclei movement. (B) A gallery plot of oosome sphericity across syncytial nuclear cycles. Color indicates relative sphericity. (C) A boxplot of sphericity values across syncytial nuclear divisions. n=20 for each nuclear cycle. Asterisks indicate significance relative to nuclear cycle 0, as assessed by Dunn's Test.
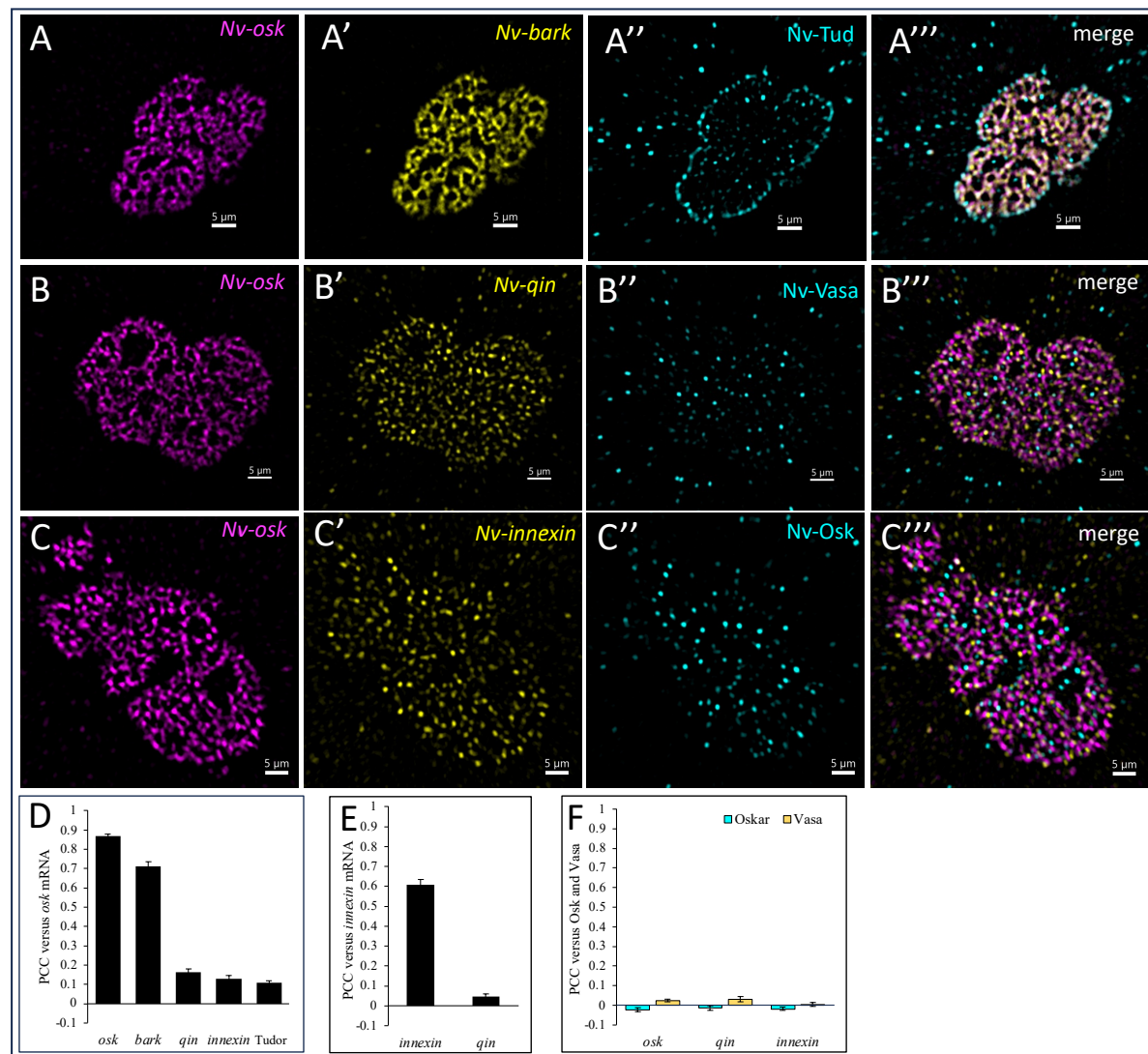
Figure 2: Oosome RNAs exhibit distinct distribution patterns depending on expression levels in the oosome, and show little co-localization with the core germ plasm proteins. (A-A''') Single plane confocal SRRF image showing the expression of Nv-osk (magenta), Nv-bark (yellow) and Nv-Tud (cyan) in oosomes. (B-B''') Single plane confocal SRRF image showing the expression of Nv-osk (magenta), Nv-qin (yellow) and Nv-Vasa (cyan) in oosomes. (C-C''') Single plane confocal SRRF image showing the expression of Nv-osk (magenta), Nv-innexin (yellow) and Nv-Osk (cyan) in oosomes. (D-F) PCC co-localization coefficients detected between oosome mRNAs stained with stellaris probes and antibody-labelled proteins (mean +/– standard error of mean, n=6-12). All scale bars, 5 μm.
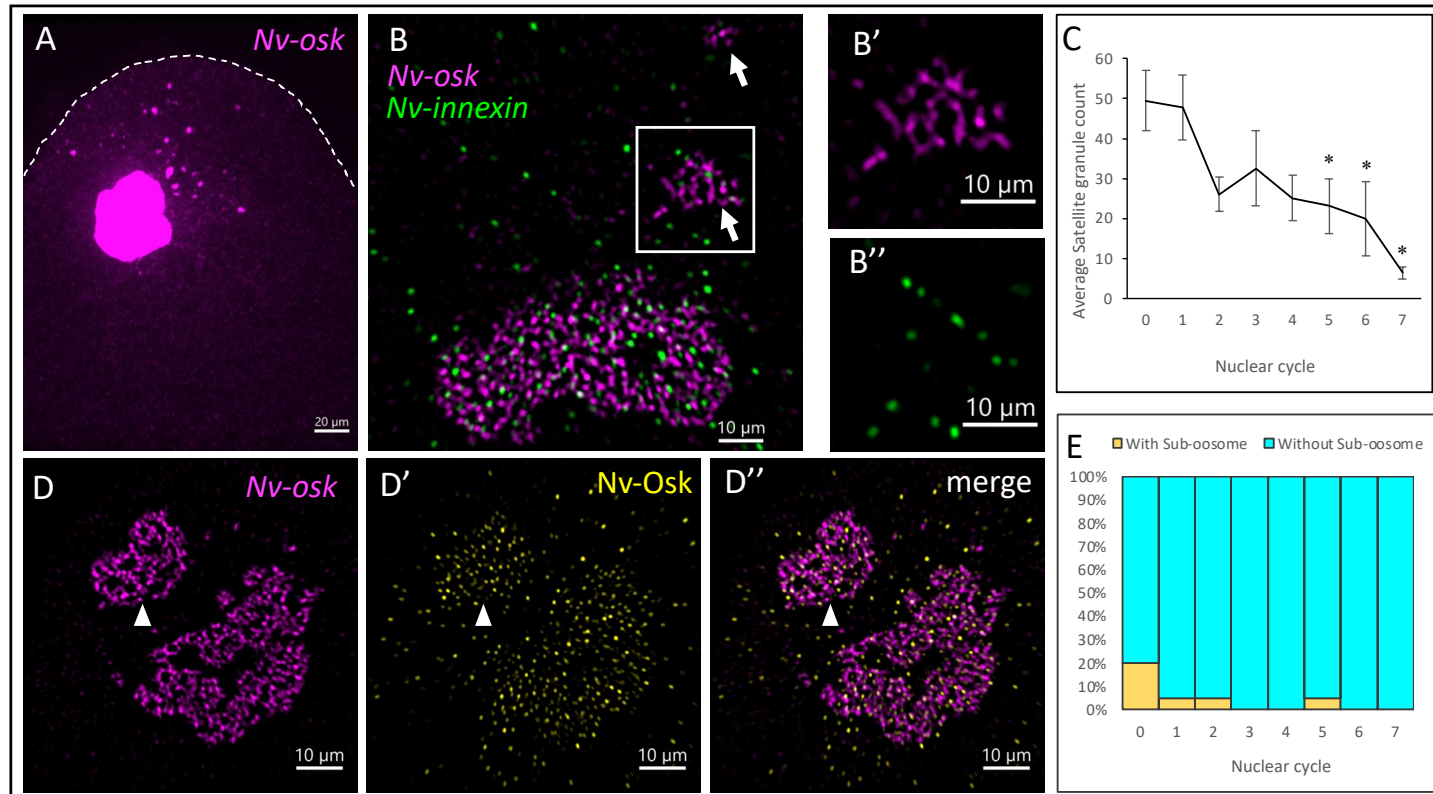
627

628

Figure 3: Smaller germ plasm aggregates (satellite particles) exist at the posterior cortex orbiting the oosome and decrease throughout the pre-blastoderm stage.

(A) Single plane confocal image of the *Nv-osk* (magenta) labeled germ plasm particles in an early-stage embryo posterior. **(B)** Single plane confocal SRRF image of the *Nv-osk* (magenta) and *Nv-innexin* (green) labeled germ plasm particles. White arrows indicate satellite particles **(B'-B")** Enlargement of the satellite particle indicated by the white box in B. **(C)** Quantification of the average number of satellite particles across syncytial nuclear cycles. Values shown are mean ± S.E.M; n = 20 embryos per nuclear cycle. Asterisks indicate statistical significance relative to before the first syncytial nuclear cleavage, as assessed by Dunn's Test. **(D-D")** Single plane confocal SRRF image of a sub-oosome labeled with *Nv-osk* (magenta) and Nv-Osk (yellow). White arrowhead indicates sub-oosome. **(E)** Quantification of sub-oosome frequency across syncytial nuclear cycles. For each nuclear cycle n=20 embryos. Scale bar in A is 20 µm. All other scale bars are 10 µm.
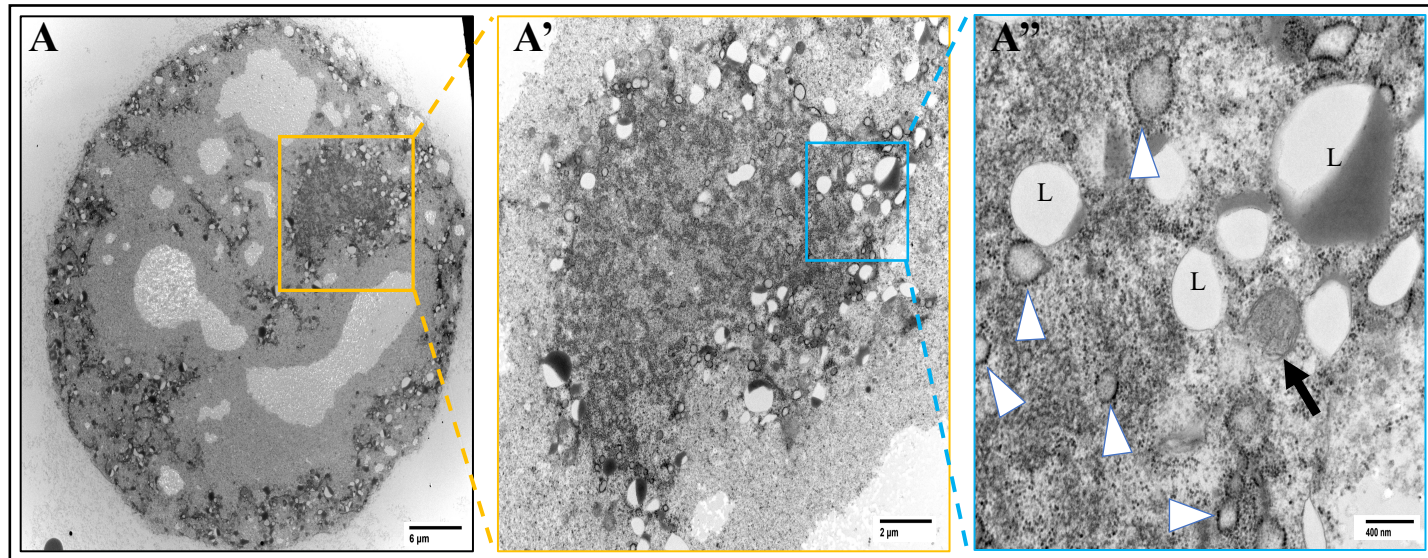
643

644

Figure 4: Oosome ultrastructure. (A) Electron micrograph of an embryo posterior
cortex containing the oosome (yellow box surrounding). Scale bar 6 μm. **(A')**
Enlargement of the yellow box containing the oosome in A. Scale bar 2 μm. **(A'')**
Enlargement of a peripheral portion of the oosome indicated by the blue box in A'. Lipid
droplets indicated with L, mitochondria with a black arrow, and RAVs with white
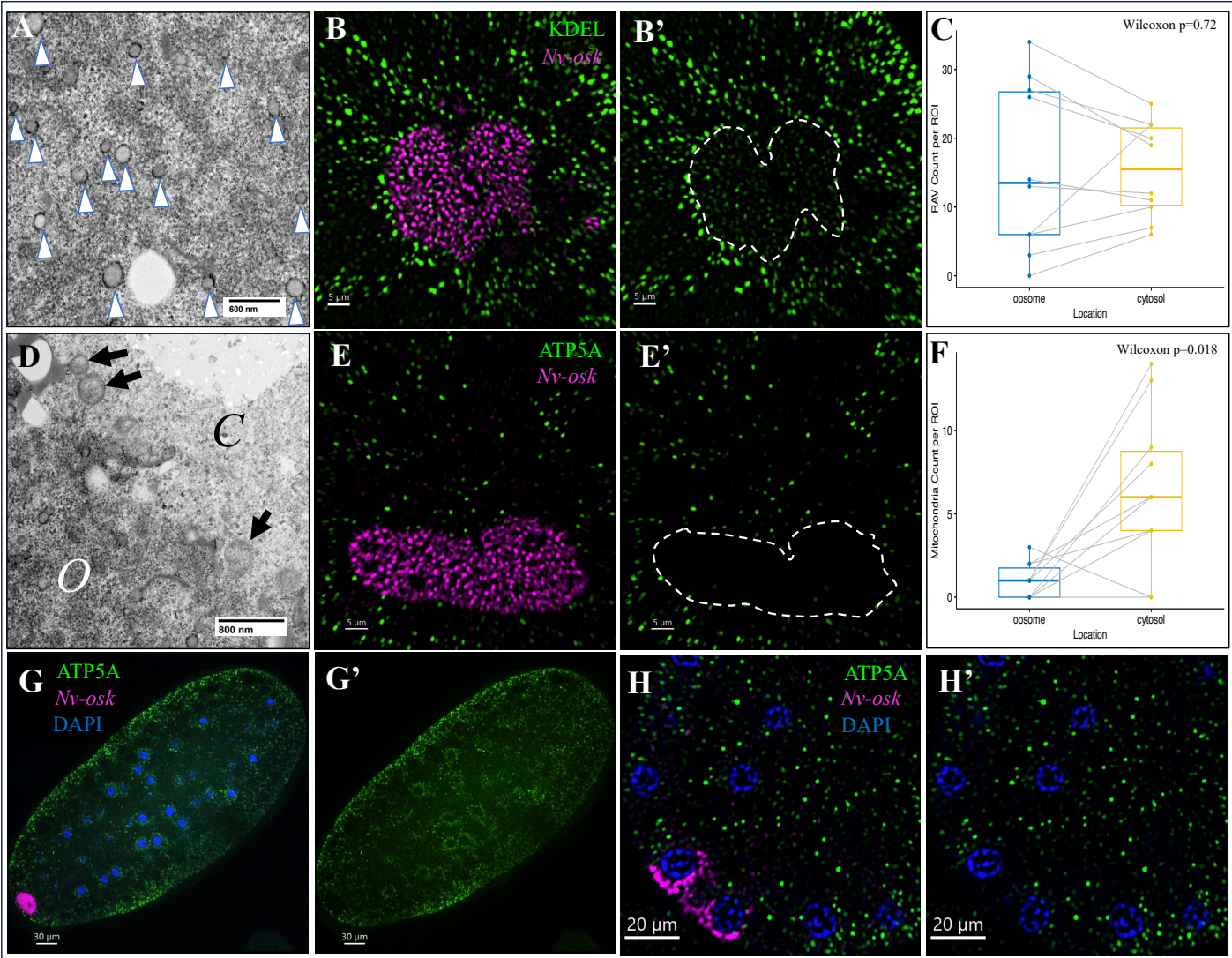arrowheads. Scale bar 400nm.

Figure 5: Oosome organelle interactions. (A) Electron micrograph of the oosome interior. Widespread RAV distribution marked with white arrowheads. Scale bar 600nm. **(B-B')** Single plane confocal SRRF image showing the distribution of RAVs within and surrounding the oosome. *Nv-osk* (magenta) marks the oosome and RAVs (green) are labeled with KDEL. Scale bars 5 μm. **(C)** Boxplots of RAV count within a segmented region of equal size both inside and just outside of the oosome. Lines between indicate pairs from the same embryo. No significant difference determined by the Wilcoxon signed rank test. **(D)** Electron micrograph of the oosome periphery. The letter O indicates the oosome and C indicates the cytosol. Black arrows mark the mitochondria at the oosome periphery. Scale bar 800nm. **(E-E')** Single plane confocal SRRF image

667   showing the distribution of mitochondria within and surrounding the oosome. *Nv-osk*

668   (magenta) marks the oosome and mitochondria (green) are labeled with anti-ATP5A.

669   Scale bars 5 µm. **(F)** Boxplots of mitochondria count within a segmented region of equal

670   size both inside and just outside of the oosome. Lines between indicate pairs from the

671   same embryo. Significant difference determined by the Wilcoxon signed rank test. **(G-**

672   **G')** Single plane confocal image showing the enrichment of mitochondria (green)

673   around nuclei (blue). Scale bar 30 µm. **(H-H')** Single plane confocal SRRF image of

674   decreased mitochondria (green) surrounding nuclei (blue) incorporated into the ooosme

675   (magenta). Scale bar 20 µm. For both organelle counts n=10 embryos.

676

677   **Acknowledgements**

681

682

683

684

685

686

687

688

689

690

691

692

693

694

695

696

697

References

1. Extavour, C.G. and M. Akam, *Mechanisms of germ cell specification across the metazoans: epigenesis and preformation.* Development, 2003. **130**(24): p. 5869-84.
2. Scholl, A., Y. Liu, and G. Seydoux, *Caenorhabditis elegans germ granules accumulate hundreds of low translation mRNAs with no systematic preference for germ cell fate regulators.* Development, 2024. **151**(13).
3. Quan, H., D. Arsala, and J.A. Lynch, *Transcriptomic and functional analysis of the oosome, a unique form of germ plasm in the wasp Nasonia vitripennis.* BMC Biol, 2019. **17**(1): p. 78.
4. Pamula, M.C. and R. Lehmann, *How germ granules promote germ cell fate.* Nature Reviews Genetics, 2024.
5. Borcherds, W., et al., *How do intrinsically disordered protein regions encode a driving force for liquid-liquid phase separation?* Curr Opin Struct Biol, 2021. **67**: p. 41-50.
6. Fung, H.Y.J., M. Birol, and E. Rhoades, *IDPs in macromolecular complexes: the roles of multivalent interactions in diverse assemblies.* Curr Opin Struct Biol, 2018. **49**: p. 36-43.
7. Krishnakumar, P., et al., *Functional equivalence of germ plasm organizers.* PLoS Genet, 2018. **14**(11): p. e1007696.
8. Lynch, J.A., et al., *The phylogenetic origin of oskar coincided with the origin of maternally provisioned germ plasm and pole cells at the base of the Holometabola.* PLoS Genet, 2011. **7**(4): p. e1002029.
9. Lehmann, R., *Germ Plasm Biogenesis--An Oskar-Centric Perspective.* Curr Top Dev Biol, 2016. **116**: p. 679-707.
10. Jones, J.R. and P.M. Macdonald, *Oskar controls morphology of polar granules and nuclear bodies in Drosophila.* Development, 2007. **134**(2): p. 233-6.
11. Ewen-Campen, B., et al., *Oskar predates the evolution of germ plasm in insects.* Curr Biol, 2012. **22**(23): p. 2278-83.
12. Kulkarni, A., et al., *oskar acts with the transcription factor Creb to regulate long-term memory in crickets.* Proc Natl Acad Sci U S A, 2023. **120**(21): p. e2218506120.
13. Blondel, L., T.E. Jones, and C.G. Extavour, *Bacterial contribution to genesis of the novel germ line determinant oskar.* Elife, 2020. **9**.
14. Ephrussi, A. and R. Lehmann, *Induction of germ cell formation by oskar.* Nature, 1992. **358**(6385): p. 387-92.
15. Kistler, K.E., et al., *Phase transitioned nuclear Oskar promotes cell division of Drosophila primordial germ cells.* Elife, 2018. **7**.
16. Trcek, T., et al., *Drosophila germ granules are structured and contain homotypic mRNA clusters.* Nature Communications, 2015. **6**(1): p. 7962.
17. Little, S.C., et al., *Independent and coordinate trafficking of single Drosophila germ plasm mRNAs.* Nat Cell Biol, 2015. **17**(5): p. 558-68.
18. Kharel, K., et al., *Dynamic protein assembly and architecture of the large solitary membraneless organelle during germline development in the wasp Nasonia vitripennis.* Development, 2024.

740 19. Hurd, T.R., et al., *Long Oskar Controls Mitochondrial Inheritance in Drosophila*
741   *melanogaster.* Dev Cell, 2016. **39**(5): p. 560-571.
742 20. Curnutte, H.A., et al., *Proteins rather than mRNAs regulate nucleation and persistence of*
743   *Oskar germ granules in Drosophila.* Cell Rep, 2023. **42**(7): p. 112723.
744 21. Banani, S.F., et al., *Biomolecular condensates: organizers of cellular biochemistry.* Nat
745   Rev Mol Cell Biol, 2017. **18**(5): p. 285-298.
746 22. Alberti, S., A. Gladfelter, and T. Mittag, *Considerations and Challenges in Studying Liquid-*
747   *Liquid Phase Separation and Biomolecular Condensates.* Cell, 2019. **176**(3): p. 419-434.
748 23. Mangiarotti, A. and R. Dimova, *Biomolecular Condensates in Contact with Membranes.*
749   Annu Rev Biophys, 2024. **53**(1): p. 319-341.
750 24. Eichler, C.E., et al., *Compartmentalized oskar degradation in the germ plasm safeguards*
751   *germline development.* Elife, 2020. **9**.
752 25. Vo, H.D.L., et al., *Protein components of ribonucleoprotein granules from Drosophila*
753   *germ cells oligomerize and show distinct spatial organization during germline*
754   *development.* Scientific Reports, 2019. **9**(1): p. 19190.
755 26. Wahiduzzaman, W., et al., *Drosophila germ granules are assembled from protein*
756   *components through different modes of competing interactions with the multi-domain*
757   *Tudor protein.* FEBS letters, 2024. **598**.
758 27. Trcek, T., et al., *Sequence-Independent Self-Assembly of Germ Granule mRNAs into*
759   *Homotypic Clusters.* Mol Cell, 2020. **78**(5): p. 941-950.e12.
760 28. Parker, D.M., et al., *mRNA localization is linked to translation regulation in the*
761   *Caenorhabditis elegans germ lineage.* Development, 2020. **147**(13).
762 29. Eno, C., C.L. Hansen, and F. Pelegri, *Aggregation, segregation, and dispersal of*
763   *homotypic germ plasm RNPs in the early zebrafish embryo.* Dev Dyn, 2019. **248**(4): p.
764   306-318.
765 30. Mahowald, A.P., *Fine structure of pole cells and polar granules in Drosophila*
766   *melanogaster.* Journal of Experimental Zoology, 1962. **151**(3): p. 201-215.
767 31. Brangwynne, C.P., et al., *Germline P Granules Are Liquid Droplets That Localize by*
768   *Controlled Dissolution/Condensation.* Science, 2009. **324**(5935): p. 1729-1732.
769 32. Folkmann, A.W., et al., *Regulation of biomolecular condensates by interfacial protein*
770   *clusters.* Science, 2021. **373**(6560): p. 1218-1224.
771 33. Mahowald, A.P., *Polar granules of Drosophila. II. Ultrastructural changes during early*
772   *embryogenesis.* Journal of Experimental Zoology, 1968. **167**(2): p. 237-261.
773 34. So, C., S. Cheng, and M. Schuh, *Phase Separation during Germline Development.* Trends
774   in Cell Biology, 2021. **31**(4): p. 254-268.
775 35. Carter, S.D., et al., *Ribosome-associated vesicles: A dynamic subcompartment of the*
776   *endoplasmic reticulum in secretory cells.* Sci Adv, 2020. **6**(14): p. eaay9572.
777 36. Tworzydło, W. and E. Kisiel, *Structure of ovaries and oogenesis in dermapterans. II. The*
778   *nurse cells, nuage aggregates and sponge bodies.* Folia Biol (Krakow), 2010. **58**(1-2): p.
779   67-72.
780 37. Bilinski, S.M., M.K. Jaglarz, and W. Tworzydlo, *The Pole (Germ) Plasm in Insect Oocytes*, in
781   *Oocytes: Maternal Information and Functions*, M. Kloc, Editor. 2017, Springer
782   International Publishing: Cham. p. 103-126.

783   38.   Martin-Solana, E., et al., *Ribosome-Associated Vesicles promote activity-dependent local*
784   *translation.* bioRxiv, 2024.

785   39.   Thomson, T., et al., *Isolation of new polar granule components in Drosophila reveals P*
786   *body and ER associated proteins.* Mechanisms of Development, 2008. **125**(9): p. 865-
787   873.

788   40.   Knaut, H., et al., *Zebrafish vasa RNA but not its protein is a component of the germ plasm*
789   *and segregates asymmetrically before germline specification.* J Cell Biol, 2000. **149**(4): p.
790   875-88.

791   41.   Czołowska, R., *The fine structure of the "germinal cytoplasm" in the egg ofXenopus*
792   *laevis.* Wilhelm Roux' Archiv für Entwicklungsmechanik der Organismen, 1972. **169**(4): p.
793   335-344.

794   42.   Chen, F., et al., *Nanoscale imaging of RNA with expansion microscopy.* Nat Methods,
795   2016. **13**(8): p. 679-84.

796   43.   Eichler, C.E., et al., *Localization of oskar mRNA by agglomeration in ribonucleoprotein*
797   *granules.* PLoS Genet, 2023. **19**(8): p. e1010877.

798   44.   Chen, R., et al., *Direct observation of translational activation by a ribonucleoprotein*
799   *granule.* Nature Cell Biology, 2024.

800   45.   Westerich, K.J., et al., *Spatial organization and function of RNA molecules within phase-*
801   *separated condensates are controlled by Dnd1.* bioRxiv, 2023.

802   46.   Putnam, A., et al., *A gel phase promotes condensation of liquid P granules in*
803   *Caenorhabditis elegans embryos.* Nat Struct Mol Biol, 2019. **26**(3): p. 220-226.

804   47.   Gatenby, J.B., *The Segregation of the Germ-cells in Tricho-gramma evanescens.* Journal
805   of Cell Science, 1918. **2**(250): p. 161-174.

806   48.   Gatenby, J.B., *Polyembryony in Parasitic Hymenoptera : A Review.* Journal of Cell Science,
807   1918. **s2-63**(250): p. 175-196.

808   49.   Buchta, T., et al., *Patterning the dorsal–ventral axis of the wasp Nasonia vitripennis.*
809   Developmental Biology, 2013. **381**(1): p. 189-202.

810   50.   Lynch, J.A. and C. Desplan, *A method for parental RNA interference in the wasp Nasonia*
811   *vitripennis.* Nature Protocols, 2006. **1**(1): p. 486-494.

812   51.   Taylor, S. and P. Dearden, *Nasonia segmentation is regulated by an ancestral insect*
813   *segmentation regulatory network also present in flies.* 2021.

814   52.   Gustafsson, N., et al., *Fast live-cell conventional fluorophore nanoscopy with ImageJ*
815   *through super-resolution radial fluctuations.* Nature Communications, 2016. **7**(1): p.
816   12471.

817   53.   Culley, S., et al., *SRRF: Universal live-cell super-resolution microscopy.* The International
818   Journal of Biochemistry & Cell Biology, 2018. **101**: p. 74-79.

819   54.   Bolte, S. and F.P. Cordelières, *A guided tour into subcellular colocalization analysis in light*
820   *microscopy.* J Microsc, 2006. **224**(Pt 3): p. 213-32.

821   55.   Costes, S.V., et al., *Automatic and quantitative measurement of protein-protein*
822   *colocalization in live cells.* Biophys J, 2004. **86**(6): p. 3993-4003.

823